



HAL
open science

Monitoring of steel-concrete bond with the acoustic emission technique

Jacqueline Saliba, Djillali Mezhoud

► **To cite this version:**

Jacqueline Saliba, Djillali Mezhoud. Monitoring of steel-concrete bond with the acoustic emission technique. Theoretical and Applied Fracture Mechanics, 2019, 100, pp.416-425. 10.1016/j.tafmec.2019.01.034 . hal-02444539

HAL Id: hal-02444539

<https://hal.science/hal-02444539>

Submitted on 22 Oct 2021

HAL is a multi-disciplinary open access archive for the deposit and dissemination of scientific research documents, whether they are published or not. The documents may come from teaching and research institutions in France or abroad, or from public or private research centers.

L'archive ouverte pluridisciplinaire **HAL**, est destinée au dépôt et à la diffusion de documents scientifiques de niveau recherche, publiés ou non, émanant des établissements d'enseignement et de recherche français ou étrangers, des laboratoires publics ou privés.



Distributed under a Creative Commons Attribution 4.0 International License

Monitoring of steel-concrete bond with the acoustic emission technique

Jacqueline Saliba

Université de Bordeaux, UMR 5295, Institut de Mécanique et d'Ingénierie (I2M), Département Génie Civil et Environnemental (GCE), 33000 Bordeaux, France

Corresponding author : jacqueline.saliba@u-bordeaux.fr

Djillali Mezhoud

Laboratoire de Génie de la Construction et Architecture (LGCA), Faculté de Technologie, Université de Bejaia, 06000 Bejaia, Algérie.

Abstract. Cracking in reinforced concrete structures is of major concern since it may affect their durability and structural integrity. Cracking is mainly influenced by stress distribution along the interface between steel and concrete which is responsible of transferring load from steel bar to the surrounding matrix. Thus, quantitative evaluation of steel-concrete bond effect on fracture properties is important. An experimental investigation on Reinforced Concrete (RC) ties is reported in this paper. Pull-out and tensile tests have been conducted on cubic specimens with high adhesion reinforcement bars with different diameters in parallel with a continuous monitoring using the Acoustic Emission (AE) and the Digital Image Correlation (DIC) techniques. Two failure modes have been observed according to the steel bar section: concrete cover splitting and pull out with damage concentrated near the concrete rebar interface. The results show a good correlation between the loading force and the AE activity with AE signal of different characteristics indicating different active fracture mechanisms. The order of appearance of cracks, their width and their spacing have been also measured in correlation with the loading level for short ties with different lengths and bar diameters.

Keywords. Steel-concrete bond, fracture of Reinforced Concrete, pull out tests, tensile tests, Acoustic Emission, Digital Image Correlation

NOMENCLATURE

RC : Reinforced Concrete

SHM : Structural Health Monitoring

AE : Acoustic Emission

DIC : Digital Image Correlation

HA : high adhesion

f_t : tensile strength of concrete

f_c : compressive strength of concrete

f_y : tensile strength of steel bar

E_s : Young modulus of steel bar

h_1 : height of the ribs

e_1 : spacing of the ribs

α_1 : angle of the ribs

α_2 : inclination of the ribs

τ_{\max} : maximum bond stress

F : maximum applied load

Φ : bar diameter

l : anchorage length

A_s : section of the steel

A_t : section of the specimen

P : the percentage of steel = A_s/A_t

c : thickness of the confinement

τ_{adh} : chemical adhesion strength

s : slip

k_s : interface shear stiffness

1. INTRODUCTION

During last years, many bridges and Reinforced Concrete (RC) structures have collapsed all over the world due to aging. In order to avoid such collapses, characterize the damage state and select a proper repair methodology, it is necessary to implement an advanced health monitoring system. The Structural Health Monitoring (SHM) offers the potential for identification of structural distress that can serve as an indicator of damage, or, in extreme cases, the distress may be a precursor to member failure or structure collapse. SHM presents different process levels: detection and localisation of damage, assessment of damage extent and, finally, prediction of the residual life of the structure [1, 2, 3].

The structural behavior of RC is highly affected by the bond between reinforcement and concrete [4]. A wide range of factors affect the bond-slip response between bars and concrete, for instances bar diameter and relative rib area [5], concrete properties, confinement effect [6, 7], bond length, reinforcing material [8 - 11], percentage of lapped bars [12] and degradation mechanisms as electrochemical chloride extraction [13] and corrosion [5, 14]. Bond-slip between reinforcement and concrete is characterized by three main components: chemical adhesion, mechanical interaction, and friction.

Two modes of bond failure are possible: pull-out and splitting of concrete cover [15, 16]. Firstly, the chemical adhesion breaks down first for low bond stress values where no slip between the reinforcement and the concrete is observed. Then, for higher bond stress values, the limited wedging action of the lugs causes transverse microcracks which allow the bar to slip.

In a bar pull-out failure, the wedging action is enhanced, and hoop stresses appear at the surrounding concrete, which at the same time exerts a confinement action on the bar. Thus, the force transfer mechanism changes from rib bearing to friction and shearing of the concrete keys cast between each pair of lugs.

In a concrete cover splitting failure, bond failure is mostly due to longitudinal splitting of the concrete surrounding the bar. Splitting cracks are present in concrete cover due to the radial pressure induced by the ribs of stressed bars.

The bond behavior is very sensitive to both the cover and the confinement [16, 17]. A recent study conducted by Mezhoud et al. [18] proposed new relationships for the characteristic values of the bond - slip law based on the same pull-out tests, and the behavior of short tie rods has been deduced.

However, few studies analyze the Acoustic Emission (AE) response corresponding to the degradation mechanisms between steel and concrete bond in order to perform a better monitoring of the fracture stage and to ensure the sustainability of RC structures [19 - 22].

The state of structure health can be determined by means of the analysis of extracted features during continuous or periodically spaced measurements. The AE technique allows real time monitoring of propagating cracks and can provide useful information about the location of defects and damage characteristics [23 - 25]. Thus, it can improve the structural safety and reduce the inspection time, the maintenance costs and the structural down-time [26].

The aim of the present work is to examine the influence of the bar diameter on the steel-concrete bond strength and splitting cracks, and to give insight on the fracture mechanisms in correlation with the AE activity. An experimental investigation on the pull-out test proposed by the RILEM [27] is reported. Pull-out and tensile tests have been conducted on cubic specimens, with different steel sections, in parallel with a continuous monitoring using resonant AE sensors and Digital Image Correlation (DIC) technique.

Firstly, the materials, the experiments and the test conditions aiming to determine the behavior of RC under pure tension are presented. Then, pull-out test results and a detailed analysis of AE signal parameters with respect to bond stress are proposed in order to characterize the different phases of failure. Finally, the influences of the reinforcement ratio, i.e. the ratio between the steel section and the cross section of the specimen, and the length of RC ties on the cracking response are investigated based on the AE and the DIC data.

2. EXPERIMENTAL PROGRAM

2.1 Materials properties

The concrete was cast using ordinary Portland cement, water, river sand and coarse aggregate with a maximum grain size of 15 mm. The mix proportion of concrete is shown in Table 1 with a water to cement ratio of 0.5.

Table 1. Concrete mixture proportions

Constituents	Dosage (kg/m ³)
Gravel 5/15	1148.07
Sand 0/5	629.34
Cement	400
Water	202.17

In order to determine the mechanical properties of concrete, compression and tensile tests have been conducted on prismatic ($15 \times 15 \times 15 \text{ cm}^3$) and cylindrical ($11 \times 22.5 \text{ cm}^3$) concrete specimens, respectively. Hot-rolled ribbed commercial steel bars have been used with a nominal diameter Φ of 8, 12, 14 and 16 mm. Table 2 presents the mechanical properties of concrete and steel bar.

Table 2: Properties of concrete and steel bar

Concrete	Mean value	Steel bar	Mean value
ft (MPa)	2.6	Es	200 GPa
fc (MPa)	33.7	fy	500 MPa

Note that the adhesion between steel and concrete depends on the geometrical characteristics of the ribs that is: the height h_1 , the spacing e_1 , the angle of the ribs α_1 (45 to 50°) and their inclination α_2 (45 to 50°) (Figure 1 and Table 3).

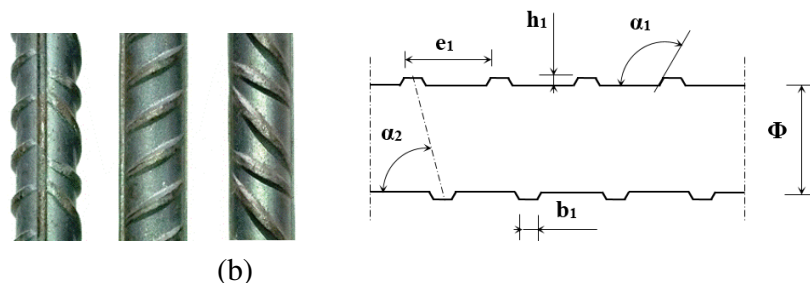


Figure 1. (a) Ribbed steel bar used (b) Geometric characteristics of the ribs

Table 3: Geometric characteristic values of the ribs

Φ (mm)	h_1 (mm)	b_1 (mm)	e_1 (mm)	A_s (mm ²)
8	0.7	0.9	5.3	50.3
12	1	1.2	7.2	1.13
14	1.1	1.4	8.4	1.154
16	1.2	1.6	9.6	2.01

2.2 Pull out tests on RC specimens

RC pull out specimens have been designed based on the RILEM [27], with a length varying in function of the bar diameter Φ . Prismatic specimens with a cross section of $100 \times 100 \text{ mm}^2$ have been used. Reinforcing steel bars have been placed before the casting of concrete, with a protective layer on the bottom and upper side of embedded steel over a length of 5Φ using a PVC hose covering, as is shown in Figure 2 (a). The protective layer avoids inaccurate stresses in the specimens and friction in the sample. Bars are embedded into concrete prism with height equal to 15Φ and the bond length of the steel bar and concrete is equal to 5Φ .

After casting, specimens have been covered with a thin sheet of plastic to prevent water loss. 24 hours after casting, specimens have been removed from the moulds and kept for curing in lime water at 20°C for 28 days.

Pull-out tests have been performed in the axial tensile mode using a testing machine with a special metal framework. The free top part of the rod has been clamped by a testing machine for pulling out and withdrawal of the reinforcing element from concrete. The sample has been placed in a holder with a stopper fixed at the lower (immobile) clamp of the testing machine (Figure 2 (b)). The sample has been loaded by pulling out the rod at a constant velocity in the vertical direction. The loading force and the displacement of the mobile clamp have been continuously monitored. Two LVDT sensors have been placed in order to measure the slip between the rod and the concrete on the bottom and the upper side of the sample, respectively.

Note that several theoretical models have been proposed in the literature to estimate the shear distribution and the ultimate shear stress at failure of steel concrete structure [28, 29]. In this study, the maximum bond stress, τ_{\max} , is considered constant along the anchorage, and is calculated as follows:

$$\tau_{\max} = F / (\pi \Phi l) \quad (1)$$

where F is the maximum applied load, Φ the bar diameter and l the anchorage length.

As the section of specimens is kept constant, the percentage of steel ρ defined as the ratio between the section of the steel (A_s) and the section of the specimen (A_t) ($\rho = A_s/A_t$) varies. The percentage ρ is equal to 0.50 %, 1.13 %, 1.54 % and 2.01 % for HA8, HA12, HA14 and HA16, respectively.

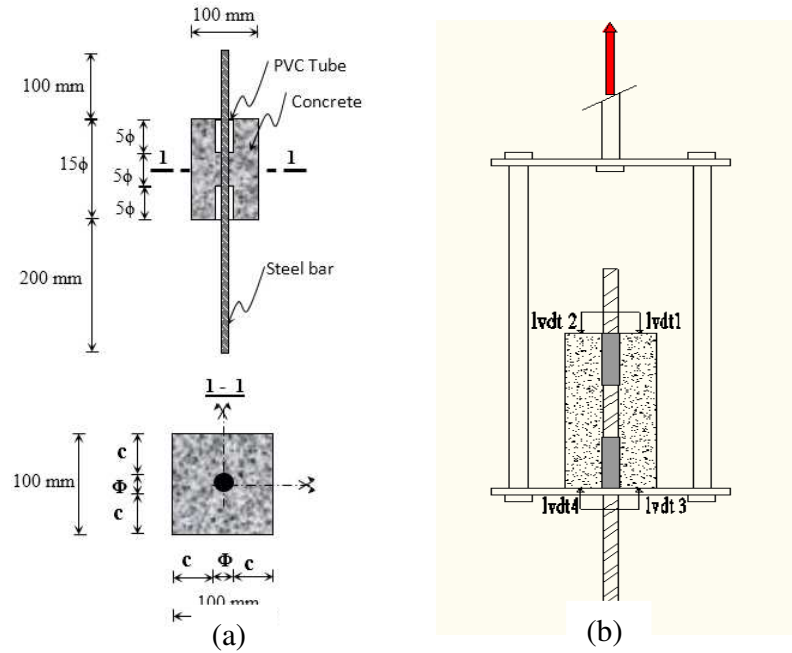


Figure 2. (a) Specimen geometry, (b) Schematic diagram of the experimental arrangement of pull-out test.

2.3 Tensile tests on RC ties

Tensile tests on RC ties have been also carried out on samples with different length and considering the same concrete cross section (that is $100 \times 100 \text{ mm}^2$) in order to study the effect of bar diameter on the state of maximum mobilization of the adhesion between steel and concrete and on the mode of decrease of this connection. For each bar diameter, three lengths have been examined: 250, 450 and 650 mm. Tensile tests have been conducted up to the yielding of the bars at a concrete age of 28 days (Figure 3). The DIC and AE techniques have been also performed during the tests.

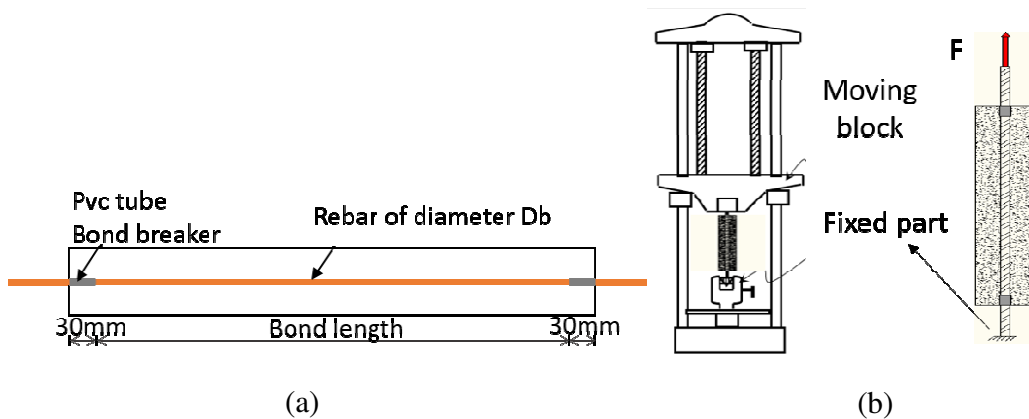


Figure 3. (a) Specimen's dimension, (b) Schematic diagram of the experimental arrangement of the tensile test

2.4 Acoustic Emission (AE) technique

The AE system consists of an eight channel AE Win system, a general-purpose interface bus (PCI-DISP4) and a PC for data storage analysis. Six piezoelectric transducers with a resonant frequency of 150 kHz have been used to convert the mechanical waves to electrical signals. Pull-out and tensile tests have been monitored by a three dimensional positioning. The sensors have been placed in 3D parallelepiped position on both free frontal surfaces of the sample with silicon grease as the coupling agent (Figure 4).

The recorded AE amplitudes range from 0 to 100 dB. The detected signals have been amplified with a 40 dB gain differential amplifier. In order to overcome the background noise, the signal detection threshold has been set at a value of about 35 dB (value adjusted before every test) slightly above the measured background noise [23]. The acquisition system has been calibrated before each test using a pencil lead break procedure HSU-NIELSEN (Norme NF EN 1330 [30]). The effective velocity and the attenuation of acoustic waves have been also calculated. For this analysis, the effective velocity is assumed to be constant for the analysis of AE source locations even though there may be some variability depending on the wave propagation path.

The effective velocity is equal to 3800 m/s. In order to eliminate mechanical and electro-magnetic disturbances, a high pass filter with a cut-off frequency of 20 kHz, and a low-pass filter with a cut-off frequency of 400 kHz have been used. Signal descriptors such as rise time, counts, energy, duration, amplitude, average frequency and counts to peak have been captured and calculated by AEwin system.

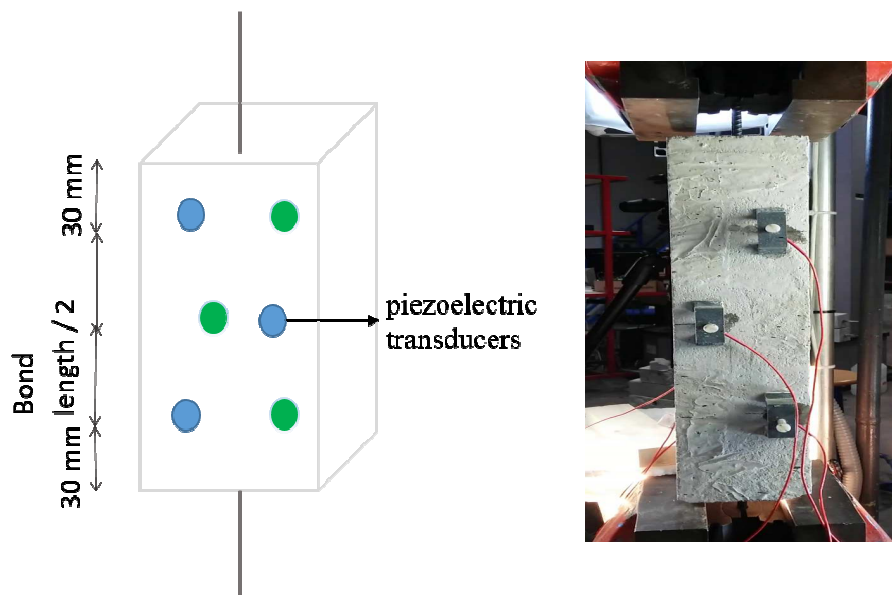


Figure 4. AE sensors arrangement

2.5 Digital Image Correlation (DIC) technique

In order to have a better understanding of the cracking process, the DIC technique has been used to measure both the cracks width and opening on the surface of the structure and the displacement field. In fact, DIC is a stable and reliable tool for fracture/damage measurement [31 - 33] with a high measurement accuracy. In addition, DIC is easy to apply experimentally and requires minimal surface preparation. The experimental procedure starts by creating a random black-and-white dot pattern on the specimen surface. White paint has been applied before the black speckle to obtain a better contrast. These patterns are then pictured using a digital camera during the loading test and stored in a computer in a digital format.

The analyses of the digital images of the deformed objects are used to estimate the in-plane displacements of various points on the surface. This methodology employs the basic continuum mechanics theory of deformation to develop and implement a procedure for estimating surface displacements. A commercial software, Vic2D, has been used in this study to perform the image correlation. During the post treatment, every zone of interest of the image is divided into several finite subsets. The correlation consists of considering a subimage in the reference image and locating that subimage in the deformed image. The size of the subsets is taken as 29 x 29 pixels which is regularly spaced in the reference image (of size 2452 x 2056 pixels) in the form of a grid.

3. PULL OUT TEST RESULTS

3.1 Load against slip curves

Figure 5 shows the load against the slip obtained for specimens with HA8, HA12, HA14 and HA16 bars. Two failure modes have been observed depending on the relationship between tensile and shear stress in concrete: concrete cover splitting with HA14 and HA16, and pull-out with damage concentrated near the concrete bar interface for HA8. Note that, for HA12, a combined failure mode has been observed and cracks have propagated at the same time longitudinally and transversally. Cracks first propagate in the concrete perpendicular to the axis of the steel rod and, as the loading increases, longitudinal cracks appear at the interface between steel and concrete surface.

Such differences are due to different confinement thickness [34] and to the interface resistance [17]. In the case of concrete cover splitting, Torre-Casanova et al. [34] established a linear relationship between the ratio τ_{\max}/f_t and the

ratio c/Φ where c represents the thickness of the confinement. From a certain critical value of c/Φ , the ratio τ_{\max}/f_t remains constant indicating a rupture by pull-out.

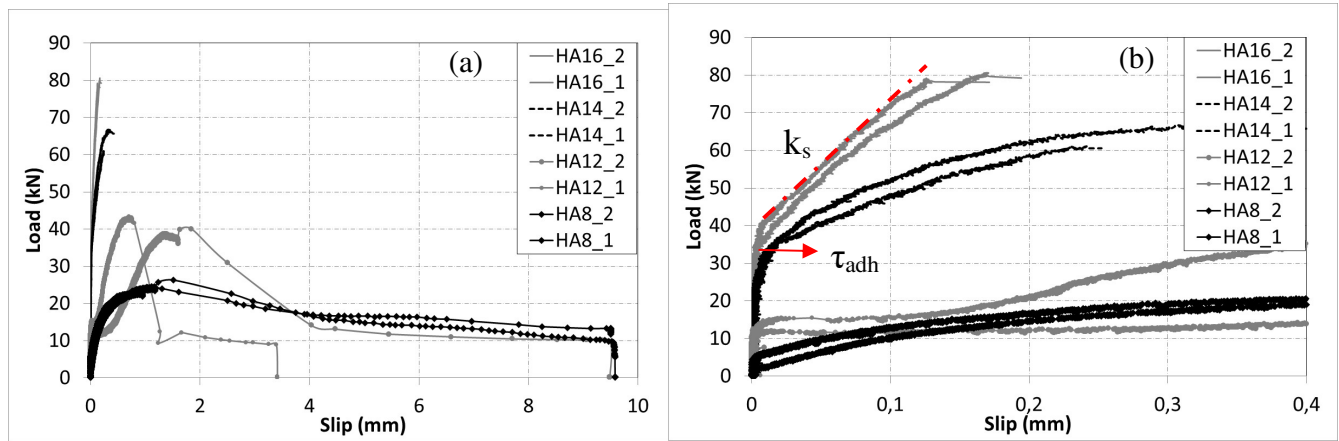


Figure 5: (a) Equivalent uniaxial behavior law of plastic sliding interface for HA8, HA12, HA14 and HA16 bars (b) zoom on the load - slip curves for low slip values.

Based on Figure 5 (b), the chemical adhesion strength τ_{adh} , which represents the ability of the interface to provide bond stress without a significant slip s , and the interface shear stiffness k_s , which is the average slope of the practically linear portion of the stress slip curve beyond the adhesion strength due to mechanical interlocking, can be calculated. The results show that both the chemical adhesion strength and the interface shear stiffness decrease with the decrease of the steel rod diameter.

Figure 6 shows the influence of both the steel rod diameter and the bond area of the embedded surface of steel rod ($S = \Pi \Phi l$) on the ultimate load. The results show that the ultimate load increases with the steel bar diameter and the embedded surface bond area by means of a nonlinear evolution.

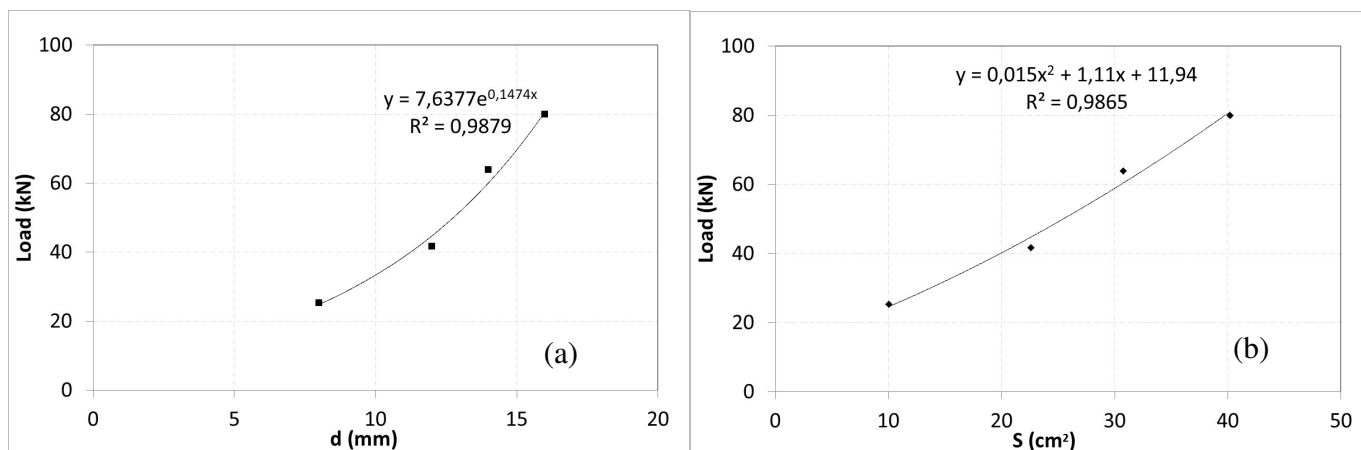


Figure 6: (a) Ultimate load versus steel rod diameter (b) Load versus embedded steel rod surface relationship.

3.2 Acoustic emission results

In order to have a better understanding of the differences between the above two modes of failure in terms of AE response, pull-out tests related to HA8 and HA16 bars have been examined. Figure 7 shows typical curves of the bond stress in correlation with the cumulative number and duration of AE hits matched on a common time scale. Three phases can be distinguished. The load increases at the beginning according to a linear law with a very low slip value (assimilated to the elastic deformation of concrete) indicating a perfect bond at the interface between concrete and steel (phase I). During this phase, few AE hits have been detected. Those hits can be attributed to the rupture of the chemical adhesion between concrete and steel.

At 20 % of the maximum strength, the AE activity begins to increase with more energetic AE hits indicating the nucleation of microcracks located along the interface between steel and concrete (phase II). This is due to the coalescence of microcracks in the zones of stress concentration related to the morphology of steel bars, the presence of the ribs and the spatial variability of the mechanical properties. In parallel, a decrease in the rigidity has been observed until the maximum value of shear stress, which corresponds to the resistance of the interface, is reached.

For HA8 specimen, shortly prior to the loss of stability, the rate of AE hits quickly increases (phase III) indicating the development of defects and the slip of the bar (Figure 7 (a)). Thus, the stress at the interface between concrete and steel bar reaches the critical stress value due to the accumulation of damage. The AE activity quickly increases after the peak with more energetic AE hits and a larger duration. Several researches have shown that the emitted AE waves and

mainly their duration are a significant characteristic of the acoustic emission source and vary as a function of the damage modes [35]. Waves of longer duration are associated to strong shearing stress and friction [20], while waves with lower duration are associated to microcracks that have a spontaneous release of energy due to tensile and compressive stress. AE signals with higher duration are accompanied with the decrease of stress indicating the slipping of the bar, the crushing of concrete between the ribs of the bar and the development of friction at the concrete-concrete and concrete-steel interface. The load decreases until the bar is displaced of a distance equal to that between the ribs. For HA16 specimen, a brittle rupture has been observed (phase III) due to the splitting of concrete accompanied with the emission of very energetic hits (Figure 7 (b)). A rapid decrease of the stress is observed indicating the loss of stability and the macroscopic rupture of concrete. The surface of the specimens after the rupture shows the traces of the ribs and the crushed concrete. The debonding failure between the concrete and the bar has been characterized by a partially peeling off of the helical wrapping layer. In fact the ribs can apply a pressure and a shear stress on the surrounding concrete; when radial cracks are extended to the surface, the splitting failure of concrete appears. Note that the number of AE hits is largely superior in the case of pull-out in comparison to that for splitting failure. This is mainly due to different damage mechanisms.

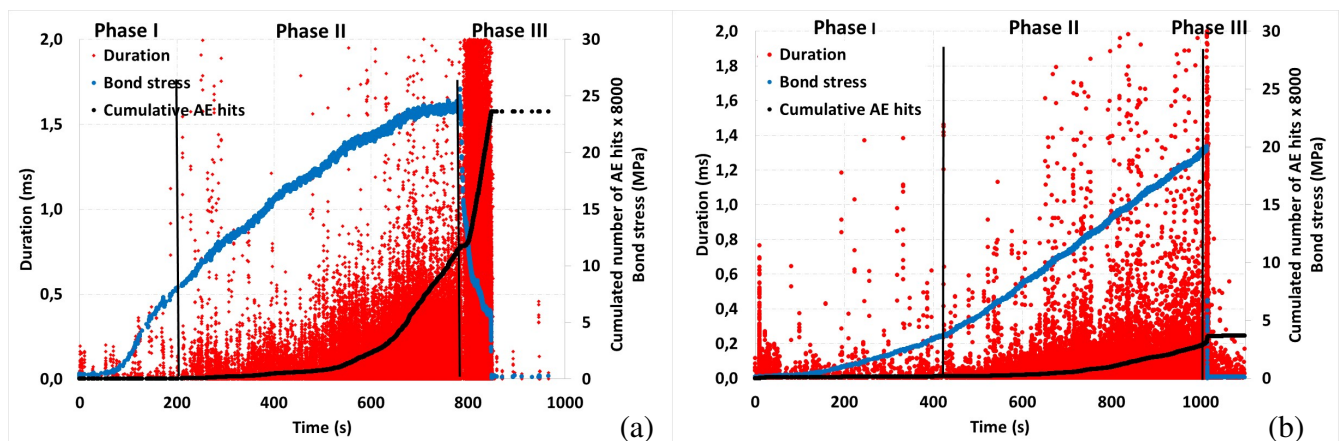


Figure 7. Correlation between the bond stress and the cumulated number of AE hits and the duration of AE hits for reinforced concrete specimens with HA8 (a) and HA16 (b) bars.

Figure 8 shows the evolution of the cumulative AE energy in correlation with the slip s between the reinforcement and the concrete against the load, for HA8 and HA16 bars. A simultaneous change of slope for both parameters has been observed indicating that the appearance of AE hits is highly related to the slipping of the bar. The acoustic emission

energy emitted during the first phase is very small, then the non-linearity appears before the maximum load due to the development of microcracking once the chemical adhesion failed. Thus, this indicates a clear correlation between damage evolution and AE parameters. For HA8 (Figure 8 (a)), high AE energy has been emitted at the peak with an important rate, indicating the degradation of the interface and the slipping of the rebar.

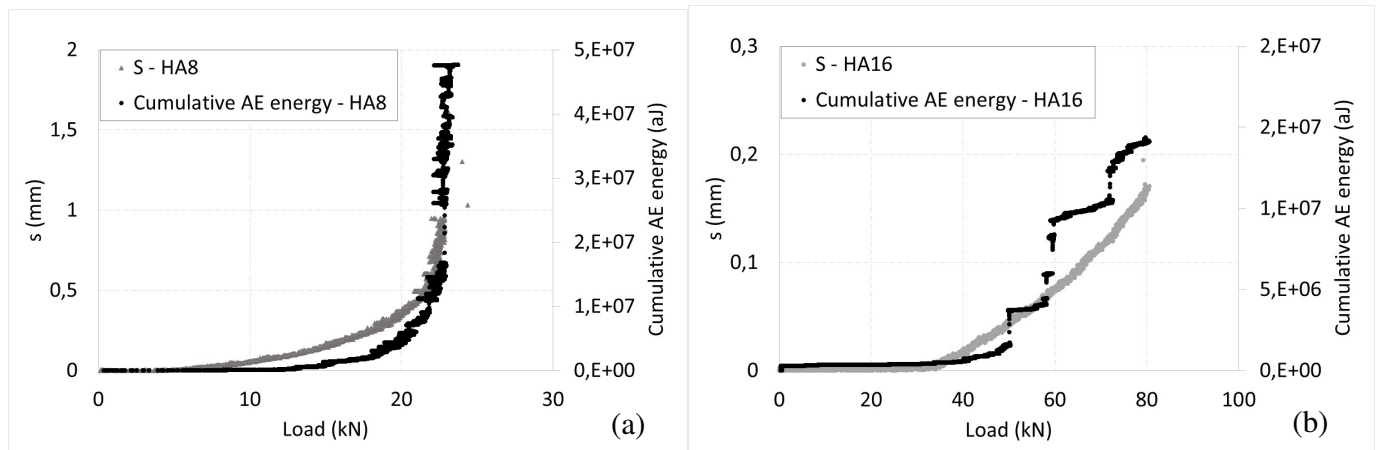


Figure 8. Evolution of the slip between the reinforcement and the concrete in correlation with the cumulated AE energy versus the load for reinforced concrete specimens with HA8 (a) and HA16 (b) bars.

3.3 Localisation maps of AE events

Figure 9 presents the localisation maps of the AE sources obtained during pull-out test. The 3D location map for HA8 rebar has been plotted. Each point corresponds to the generation of a microcrack in the specimen. The total number of AE events is very important with more than 14000 events. For a better evaluation of damage, the 2D localisation map of the cross section of the specimen has been plotted and different levels of energy have been considered over a window in function of the position X and Z centered at the bar. The position of the rebar can be seen clearly at the center of the section. In addition, the density of AE events and their energy are much more important on the sides of the bar (where the ribs are present) due to the coalescence of microcracks in the zones of stress concentration. A stress variation in the load transfer between steel and surrounding concrete can also be observed.

The 2D location map of AE events have been also studied along the bar length in function of the position Y and X (Figure 9 (c)). Events with different levels of energy, concentrated along the bond length mainly at the interface between steel and concrete due to concrete damage and the friction at the concrete-concrete and concrete-steel interface,

have been observed. Note that the distribution of AE events along the length of the bar (Figure 9 (d)) shows that the stress distribution along the transfer length in the pull-out tests is not constant and is influenced by the properties of the interface and the bond stress relationship. The results show that the damage is located in the vicinity of the applied load and diffused proportionally in the interior of the specimen.

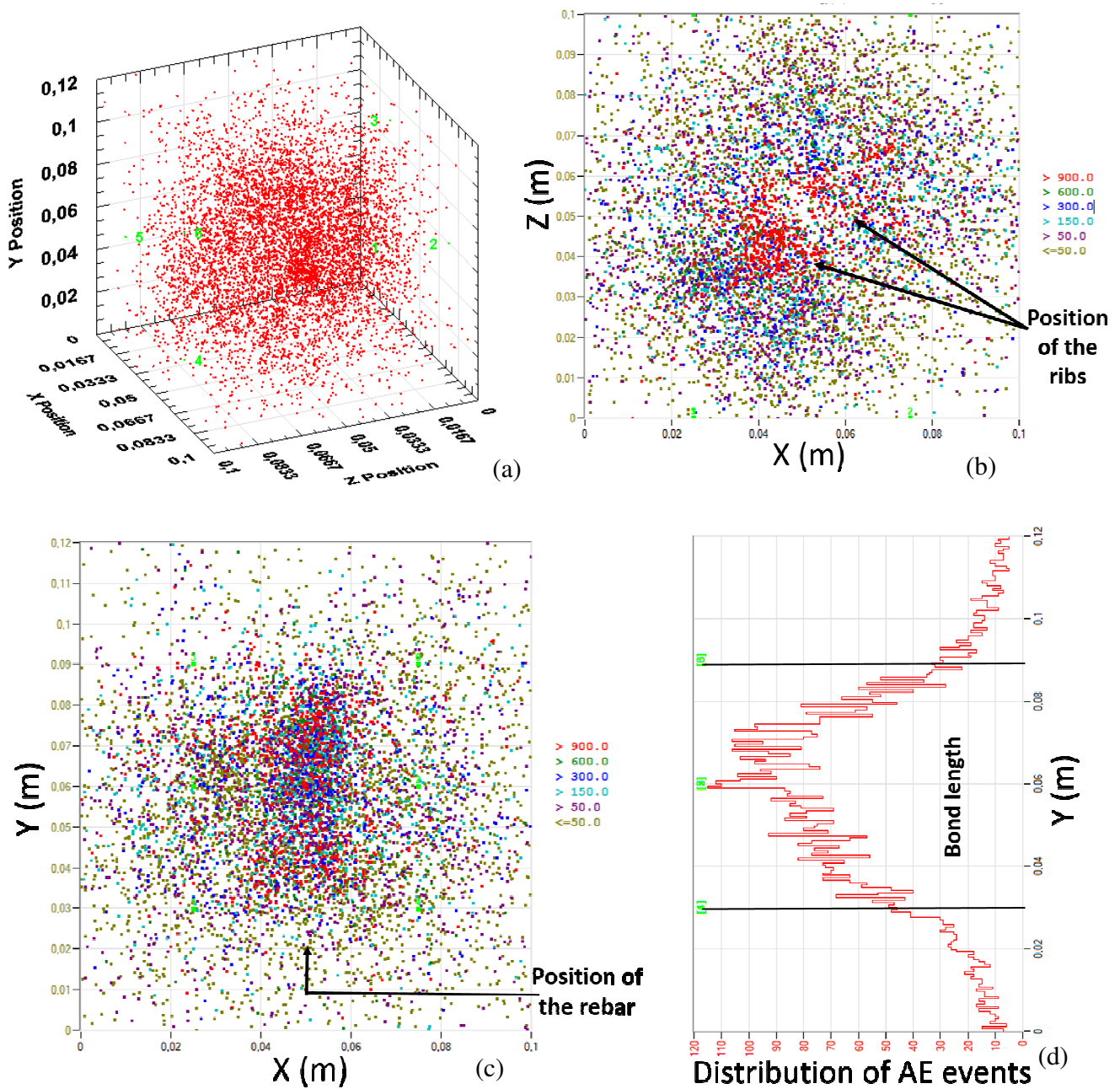


Figure 9. (a) 3D localisation map of AE events, (b) projection along the plan XZ, (c) projection along YX and, (d) the corresponding distribution along Y for reinforced concrete specimens with HA8.

The damage localisation maps of acoustic emission events have been also plotted for cover splitting failure (Figure 10). The total number of AE events is weak (750 events) generated in comparison with pull-out rupture tests. For cover splitting failure, the detected AE events are more dispersed with events of higher energy located at the zone of macrocrack. Few AE events have been emitted during the splitting due to the brittle behavior.

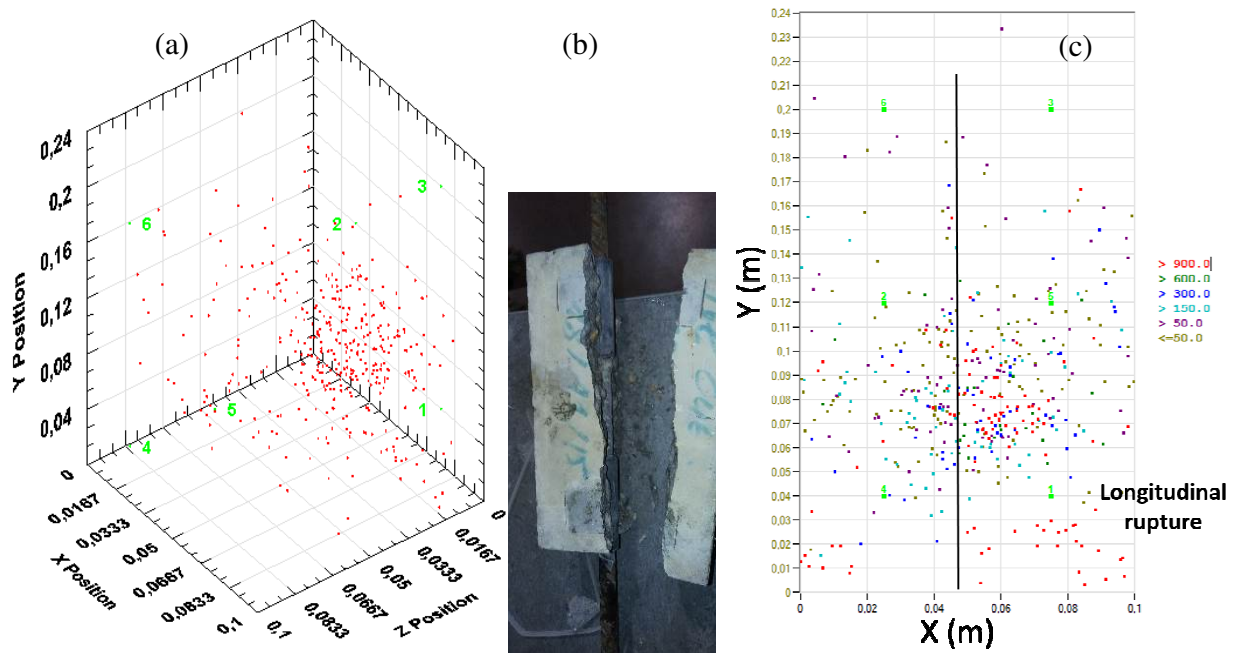


Figure 10. (a) 3D localisation map of AE events, (b) detail of the splitting crack, (c) projection along YX for reinforced concrete specimens with HA16.

4. TENSILE TEST RESULTS

4.1 Stress - strain curves

Tensile tests on RC ties is one of the most suitable tests for observing the propagation of cracks in RC structures [36, 37]. As the specimen is subjected to pure tension loading, the effects of the steel and concrete bond, such as stress distribution, tension stiffening reduction and concentration of forces at some local points, can be observed. The behavior of short ties under tensile tests can be decomposed in three phases: an elastic linear phase; a phase of development of cracking characterized by a progressive increase of cracks along the tie rod and a decrease in structural rigidity; finally a stabilized cracking phase for which the behavior of the tie rod is governed by the behavior of the steel. The stress-strain curves of RC ties of a length of 250 mm with HA8 and HA16 bars are plotted in Figure 11 based on

the control of the displacements of several targets placed on the ties surface. For HA8, the adhesion in the tie rod increases linearly up to a normal stress in the steel rod of 319 MPa. From this level of loading, the slope considerably decreases and the modulus of elasticity of the tie rod is slightly greater than that of the steel bar. For HA16, the adhesion between the steel and the concrete in the tie rod increases linearly up to 106 MPa, then a reduction in the slope is observed due to the deterioration of the adhesion up to the elastic limit stress of the steel [18].

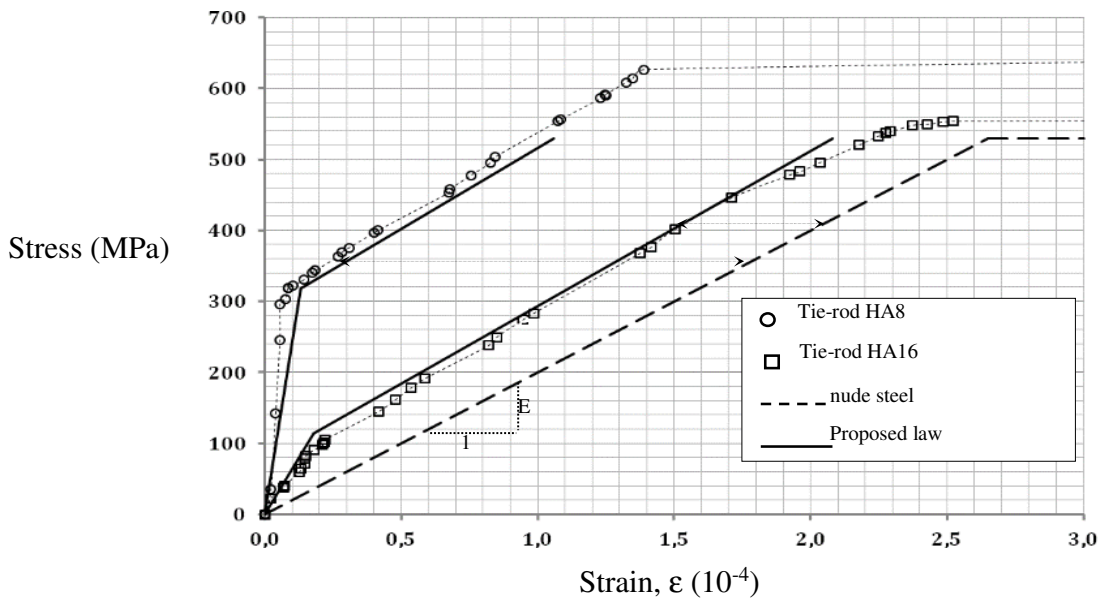


Figure 11. Stress-strain curves of tie-rods with HA8 and HA16 bars.

In function of the bar diameter and the length of the ties, different numbers of main cracks have been observed during tensile tests. The behavior of the ties is actually governed by the interaction between steel and concrete along the interface. During the elastic phase, the elongation of short ties is progressive with the applied load. At the ends of the tie rod, the load is entirely supported by the steel rod. The load is then transferred to both materials along a transfer length until the load is perfectly distributed. Stresses in concrete increase with loading until the stress is equal to the maximum strength of concrete where the tensile strength is weak considering the heterogeneity of concrete.

When RC ties are cracked, stresses are equal to zero locally and the load is totally supported by steel. On both sides of the crack, stresses are again progressively transferred to concrete due to bond adhesion. The stress increases in concrete far from the crack until the stresses are again homogeneous in both materials. After the formation of the first primary crack, a second generation of primary cracks occurs for a somewhat higher load level. The minimum distance between

the cracks is determined by analyzing the progressive cracking of the member and its subdivision into smaller parts. A stabilized crack pattern is attained when the length of a single part is no longer sufficient to allow the concrete strain to reach the failure value in tension.

Table 4 shows the number of cracks obtained in function of the bar diameter and the length of the RC ties. The number of transverse cracks increases with the length of the ties and the bar diameter. No cracks have been observed with the ties of a length of 250 mm while the number of cracks increases from 1 to 2 and 3 for HA8, HA12 and HA14 and HA16, respectively. Stress distribution is related to the transfer of bond forces from steel to concrete. Crack appearance is thus induced by the stress redistribution along the transition zone and the distribution of the tensile strength along the tie related to the heterogeneous characteristics of concrete [34]


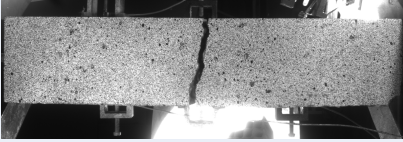
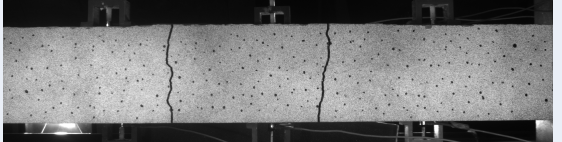
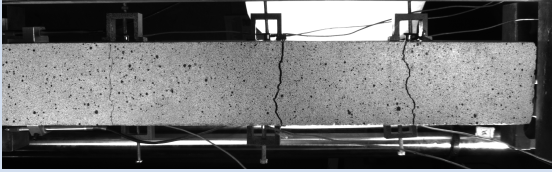
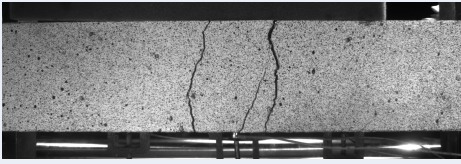
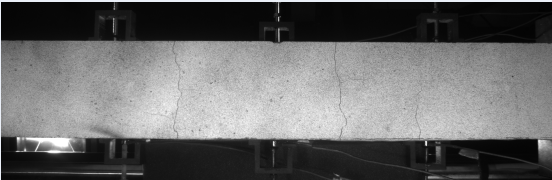
L (mm)	250	450	650
HA8	0	0	1 
HA12	0	1 	2 
HA14	0	1	3 
HA16	0	2 	3 

Table 4: Number of cracks in function of both bar diameter and length of RC ties.

4.2 Monitoring of short ties with the AE technique

Tensile tests have been also monitored with the AE technique. Figure 12 shows the evolution of the applied load in correlation with the cumulative number of AE hits and the duration of AE hits matched on a common time scale for reinforced concrete specimen with HA8 and HA16 bars and a length of 650 mm. Monitoring of short ties with the AE technique allows to distinguish the different phases of damage in RC structures. AE signals with parameters similar to those generated during pull-out tests has been also observed at different loading levels indicating similar damage mechanisms.

Few AE signals are firstly detected due to the rupture of the chemical adhesion between concrete and steel, then AE hits increase with loading due to the generation of microcracking in concrete. A sudden increase of the number AE hits is observed indicating the development of a macrocrack; this is accompanied with the generation of AE hits of high duration and energy. The number of AE hits continues to increase indicating the microcracking of concrete up to the development of secondary cracks in the case of HA16. Then, the number of AE hits increases with a higher rate indicating that steel bars have attained the elastic limit stress accompanied with AE hits of higher duration.

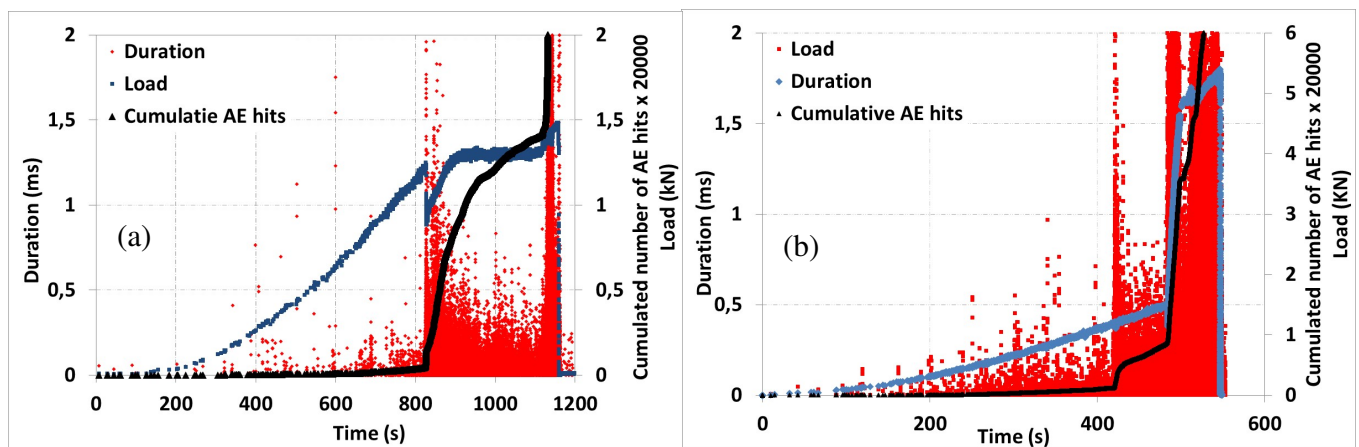


Figure 12: Correlation between the tensile stress and the cumulated number of AE hits and the duration of AE hits for reinforced concrete specimens with HA8 bar (a) and HA16 bar (b) and a length of 650 mm.

Figure 13 shows the cumulative number of AE hits for RC ties with different bar diameters and different lengths. The same phases can be observed with few AE hits corresponding to the uncracked condition of the ties. Then, the number of AE hits slightly increases up to the development of the macrocrack which can be identified by the sudden decrease of the load. The number of AE hits continue to increase up to the plastification of steel which is characterized by an

important rate of AE hits. The results show that the AE activity is more important with bars of higher diameters due to the higher bond surface.

The effect of the length of the ties can be also distinguished clearly (Figure 13 (b)). The AE activity with ties of length of 250 is very weak indicating that this length is not enough for a continuous transfer of loading from the steel bar to the concrete. For higher lengths, the number of AE hits increases indicating the development of damage and transverse cracking up to the rupture of steel bars.

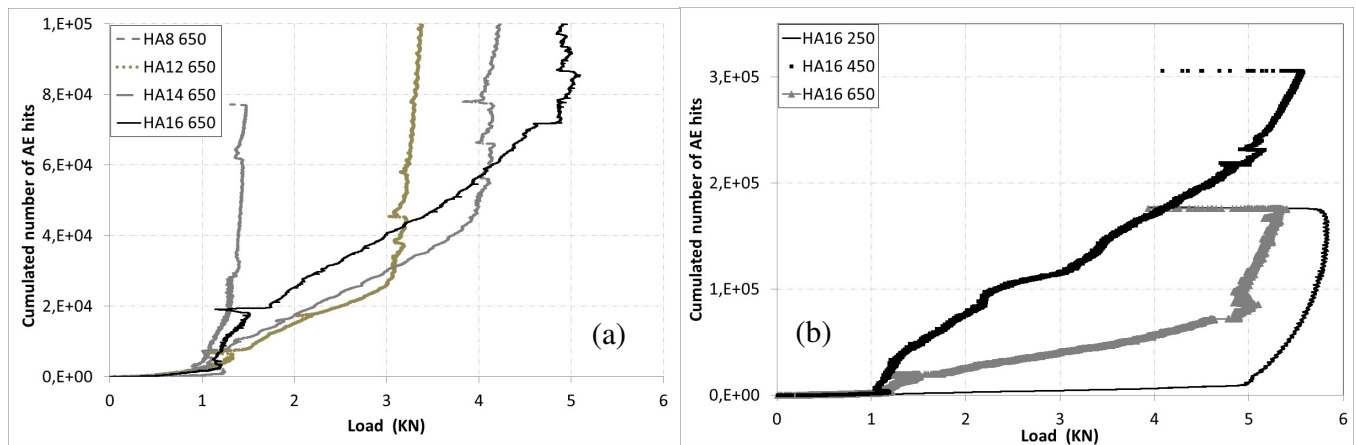


Figure 13: Cumulated number of AE hits versus the load for RC ties (a) effect of bar diameters (b) effect of RC ties length.

4.2 Damage localisation

Figure 14 shows the AE events localisation maps in correlation with the DIC at different loading levels for RC concrete ties with HA16 bar and length of 650 mm. The number of cracks increases with loading up to stabilization. At the end, ties comprises a finite number of cracks regularly distributed along the tie rod. However, for RC ties with HA16, i.e. with a percentage of steel of 2.01%, as more load has been applied beyond the cracking load, a combination of transverse and splitting cracking has been observed. Note that once the cracking process stabilizes, no more new cracks appear and only opening of the existing cracks is observed.

The cracking patterns of the reinforcement are presented in the deformation field of the studied 2D surface. Based on such images, the order of appearance of transverse cracks, their width and their spacing can be measured. In addition, the location of AE events is consistent with actual crack development obtained through

DIC. The number of AE event increases very rapidly with a higher energy due to the development of macrocracks and, as the loading increases, numerous cracks appear along the length of RC ties accompanied with the apparition of AE events.

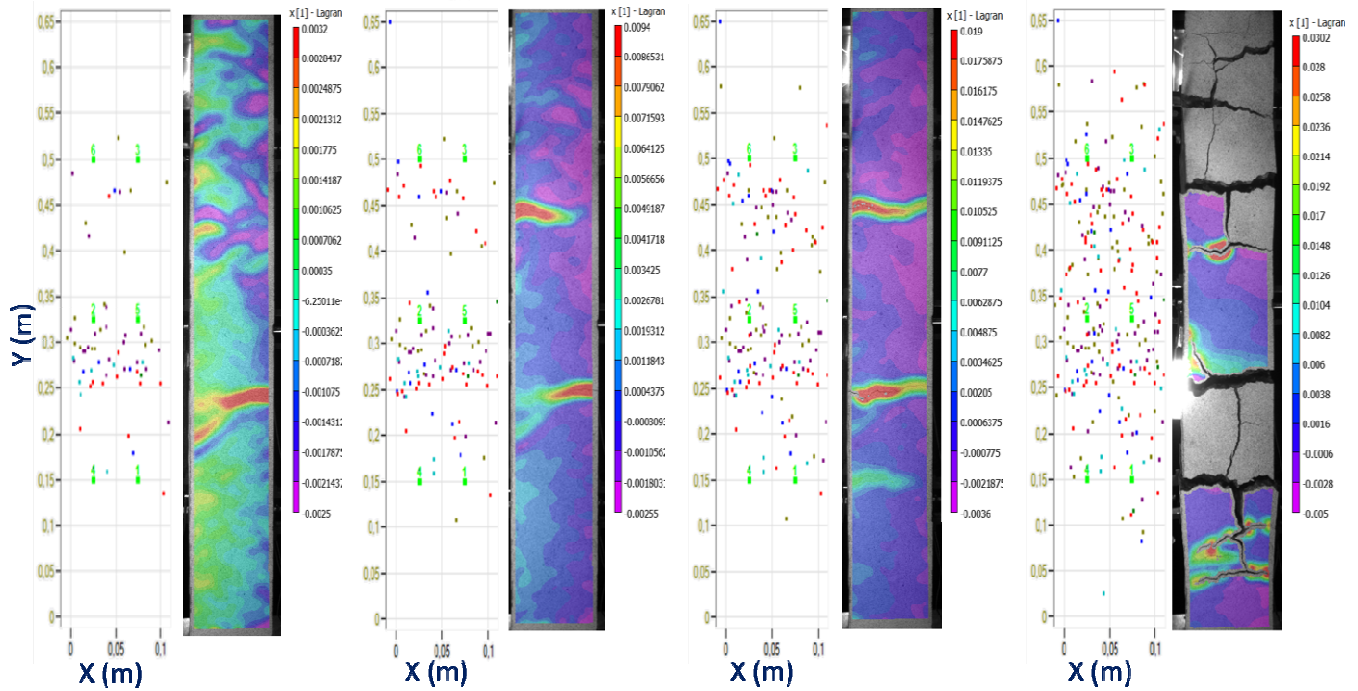


Figure 14: AE events localisation maps in correlation with the vertical displacement obtained with DIC at different loading levels

5. CONCLUSIONS

The present research study allows to analyze the characteristics of AE hits generated during pull-out and tensile tests of RC ties. Two modes of failure are observed in function of the bar diameter: pull-out and splitting of concrete failure. The AE activity is highly correlated to different degradation states of steel-concrete bond. The pull-out failure generates a high number of AE signals characterized with important duration due to friction in comparison to the brittle splitting fracture with a macroscopic longitudinal crack. A good correlation is observed between the cumulative number of AE hits and AE energy with the slip, i.e. the steel concrete degradation with the micro and macrocracking stages. Tensile tests have been also conducted in order to investigate the cracking response of RC structures and the influence of the

steel percentage. AE analysis enables the detection of the early stage of bond deterioration, the development of microcracking and the identification of the macrocracking prior to the plastic deformation of steel. The order of apparition of transverse cracks, their width and their spacing have been measured with DIC, and the AE activity response has been analyzed. Numerical simulation will be realized in future studies for a better understanding of the influence of different properties and parameters on the steel – concrete bond and for reduction of the amount of experiments.

6. REFERENCES

- [1] O. Yapar, P.K. Basu, P. Volgyesi, A. Ledeczki, Structural health monitoring of bridges with piezoelectric AE sensors. *Engineering Failure Analysis* 56 (2015) 150-169.
- [2] F. Sagasta, M.E. Zitto, R. Piotrkowski, A. Benavent-Climent, E. Suarez, A. Gallego, Acoustic emission energy b-value for local damage evaluation in reinforced concrete structures subjected to seismic loadings. *Mechanical Systems and Signal Processing* 102 (2018) 262-277.
- [3] E. Verstrynghe, K. De Wilder, A. Drougkas, E. Voet, K.V. Balen, M. Wevers, Crack monitoring in historical masonry with distributed strain and acoustic emission sensing techniques. *Construction and Building Materials* 162 (2018)898-907.
- [4] L. Jason, A. Torre-Casanova, L. Davenne, X. Pinelli, Cracking behavior of reinforced concrete beams : experiment and simulations on the numerical influence of the steel-concrete bond. *International Journal of Fracture* 180 (2013) 243-260.
- [5] G. Metelli, G. A. Plizzari, Influence of the relative rib area on bond behavior, *Magazine of Concrete Research*, 66 Issue 6, (2014) 277-294
- [6] C.A. Issa, J.J. Assaad, Bond of tension bars in underwater concrete: effect of bar diameter and cover. *Materials and Structures*. 48(11) (2015) 3457-3471.
- [7] A. Torre-Casanova, L. Jason, L. Davenne, X. Pinelli, Confinement effects on the steel – concrete bond strength and pull out failure, *Engineering Fracture Mechanics*, 97 (2013) 92-104
- [8] M. Baena, L. Torres, A. Turon, C. Barris, Experimental study of bond behaviour between concrete and FRP bars using a pull-out test. *Composites Part B* 40 (2009) 784-797.
- [9] D. Novidis, S.J. Pantazopoulou, E; Tentolouris, Experimental study of bond of NSM-FRP reinforcement. *Construction and Building Materials* 21 (2007) 1760-1770.
- [10] L. Bouazaoui, A. Li, Analysis of steel/concrete interfacial shear stress by means of pull out test, *International Journal of Adhesion & Adhesives* 28 (2008) 101-108
- [11] U.K. Sharma, P. Bhargava, S.A. Sheikh, Tie-confined fibre-reinforced high-strength concrete

- columns, Magazine of concrete Research, 59(10) (2007) 757-769.
- [12] G. Metelli, J. Cairns, G. Plizzari, The influence of percentage of bars lapped on performance of splices. *Materials and Structures* 48 (2015) 2983-2996.
- [13] N.M. Ihekweba, B.B. Hope, C.M. Hansson, Pull-out and bond degradation of steel rebars in ECE concrete. *Cement and Concrete Research*. 26(2) (1996) 267-282.
- [14] S.P. Tastani, S.J. Pantazopoulou, Behavior of corroded bar anchorages, *ACI Structural Journal*, 104(6) (2007) 756-766
- [15] E. Baran, T. Akis, S. Yesilmen, Pull-out behavior of prestressing strands in steel fiber reinforced concrete, *Construction and Buildings Materials* 28 (2012) 362-371
- [16] G.A Plizzari, M.A. Deldossi, S. Massimo, Experimental study on anchored bars in R.C. elements with transverse reinforcement, *Materials and Structures*. 29 (1996) 534-542.
- [17] P.G. Gambarova, G. Rosati, Bond and splitting in reinforced concrete: test results on bar pull-out, *Materials and Structures*, 29 (1996) 267-276.
- [18] D. Mezhoud, Y. Bouafia, M. Saad, J. Saliba, Bond-slip law and short tie behavior without main cracks, *Journal of Adhesion Science and Technology*, <https://doi.org/10.1080/01694243.2018.1432235>
- [19] W. Lei, Y. Jin, X. Hailong, F. Lei, Experimental study of a pull-out test of corroded steel and concrete using the acoustic emission monitoring method, *Construction and Building Materials* 122 (2016) 163-170
- [20] C.U.Grosse, H.W. Reinhardt, G. L. Balazs, Acoustic emission data from pull-out tests of reinforced concrete analysed with respect to passive US-Tomography, *Acoustical imaging*. 21 (1995) 635-647.
- [21] M.N. Noorsuhada, An overview on fatigue damage assessment of reinforced concrete structures with the aid of acoustic emission technique. *Construction and Building Materials*. 112 (2016) 424-439.
- [22] I. Dakanali, I. Stavrakas, D. Triantis, S.K. Kourkoulis, Pull-out of threaded reinforcing bars from marble blocks, *Procedia Structural Integrity* 2 (2016) 2865-2872.
- [23] J. Saliba, M. Matallah, A. Loukili, J.P. Regoin, D. Grégoire, L. Verdon, G Pijaudier-Cabot, Experimental and numerical analysis of crack evolution in concrete through acoustic emission technique and mesoscale modelling, *Engineering Fracture Mechanics*, 167 (2016) 123–137.
- [24] J. Saliba, A. Loukili, J.P. Regoin, D. Grégoire, L. Verdon, G. Pijaudier-Cabot, Experimental analysis of crack evolution in concrete by the acoustic emission technique, *Fracture and structure integrity*. 34 (2015) 331-339.
- [25] A. Boniface, Z.M. Sbartaï, J. Saliba, N. Ranaivomanana, Comparison of localization strategies of damage in concrete by acoustic emission, *NDT.net issue*. 21(11) (2016).

- [26] Carpinteri A., Lacidogna G., Pugno N., "Structural damage diagnosis and life-time assessment by acoustic emission monitoring", *Engineering Fracture Mechanics*, vol. 74, p. 273-289, 2007.
- [27] RILEM, Essais portant sur l'adhérence des armatures du béton :2 : Essai par traction, *Materials and structures*, 03 (1970) 175-178.
- [28] A. A. ABouhoussein, A.A. Hassan, Acoustic emission-based analysis of bond behavior of corroded reinforcement in existing concrete structures. *Structural Control and Health Monitoring*. 24 (2017) e1893
- [29] S. Khalafallah, Modeling of bond for pull-out tests. *Building Research Journal*. 56 (2008) 37-48
- [30] Norme NF EN 1330-9. Essais non-destructifs - Terminologie - Partie 9 : Termes utilisés en contrôle par émission acoustique. AFNOR, 2009.
- [31] S. Y. ALAM, J. Saliba, A. Loukili, Digital image correlation and acoustic emission: a simultaneous approach for fracture examination in concrete, *Construction & Building Materials*. 69 (2014) 232-242.
- [32] F. Hild, S. Roux, Digital Image Correlation: from Displacement Measurement to Identification of Elastic Properties – a Review, *Strain*. 42(2) (2006) 69-80.
- [33] L.-P. Guo, W. Sun, A. Carpinteri, Latent crack path and service life predictions for unnotched concrete under bending by digital speckle correlation method. *Fatigue and Fracture of Engineering Materials and Structures* 31 (1) (2008) 29-37
- [34] Torre-Casanova A., Jason L., Davenne L., Bond slip model for the simulation of reinforced concrete structures, *Engineering Structures*, 39 (2012) 66-78.
- [35] A.C. Mpalaskas, I. Vasilakos, T.E. Matikas, H.K. Chai, D.G. Aggelis, Monitoring of the fracture mechanisms induced by pull-out and compression in concrete. *Engineering Fracture Mechanics*. 128 (2014) 219-230.
- [36] T.S. Phan, P. Rossi, J.L. Tailhan, Numerical modelling of the concrete/rebar bond, *Cement & Concrete Composites* 59 (2015) 1-9.
- [37] A. Michou, A. Hilaire, F. Benboudjema, G. Nahas, P. Wyniecki, Y. Berthaud, Reinforcement-concrete bond behavior: Experimentation in drying conditions and meso-scale modeling. *Engineering Structures* 101 (2015) 570-582.